Determining Modes and Grashof Number in 2D Turbulence—A Numerical Case Study

Eric Olson[1,2] and Edriss S. Titi[3,4,5]

We study how the number of numerically determining modes in the Navier–Stokes equations depends on the Grashof number. Consider the two-dimensional incompressible Navier–Stokes equations in a periodic domain with a fixed time-independent forcing function. We increase the Grashof number by rescaling the forcing and observe through numerical computation that the number of numerically determining modes stabilizes at some finite value as the Grashof number increases. This unexpected result implies that our theoretical understanding of continuous data assimilation is incomplete until an analytic proof which makes use of the non-linear term in the Navier–Stokes equations is found.

1. Introduction

In the 1960s the theory of determining modes was introduced by Foias and Prodi [19]. The method of continuous data assimilation was proposed at about the same time by Charney, Halem and Jastrow [7] to process satellite data and obtain improved estimates of the current atmospheric state. Continuous data assimilation was used by Browning, Henshaw and Kreiss [3,4] and Henshaw, Kreiss and Ystrröm [24] to study decaying turbulence in the two-dimensional incompressible Navier–Stokes equations. In [28] the connection between continuous data assimilation and the theory of determining modes was made clear.

The idea behind continuous data assimilation is to feed observational data into a model as it is being integrated in time so that an approximate solution converges to the true solution. In the mathematical setting considered here, we use continuous data assimilation to construct two solutions to the two-dimensional Navier–Stokes equations that satisfy the hypothesis of the theory of determining modes. Thus, the theory of determining modes guarantees that the approximate solution obtained by continuous data assimilation converges to the true solution over time provided enough Fourier modes are used as observational data. We compare existing mathematical bounds and intuition to numerical results from a number of continuous data assimilation experiments.

[1] Department of Mathematics, Indiana University, Bloomington IN 47401, USA

[2] Department of Mathematics, University of Nevada, Reno NV 89557, USA

[3] Department of Mathematics, University of California, Irvine CA 92697, USA

[4] Mechanical and Aerospace Engineering, University of California, Irvine CA 92697, USA

[5] Department of Computer Science and Applied Mathematics, Weizmann Institute of Science, Rehovot 76100, Israel

In our previous work [28] we studied how continuous data assimilation and the number of determining modes in the two-dimensional Navier–Stokes turbulence are affected by the spatial length scales present in the body forcing f. In this work we keep the spatial structure of the forcing function fixed and vary the Grashof number by varying the amplitude of the forcing function. Namely, we vary the Grashof number by rescaling the forcing function by a multiplicative factor γ. This is equivalent to changing the viscosity or the size of the domain. As γ increases, or equivalently as the viscosity ν decreases, the turbulent flow becomes more energetic and one would expect the number of numerically determining modes to increase as well. This intuition is supported by existing theoretical bounds on the number of determining modes and the dimension of the global attractor given in Foias, Manley, Rosa and Temam [18] and references therein. In particular, the best available upper bounds on the number of determining modes, nodes and finite-volume elements given in [9] and [26] all increase as the viscosity decreases. Similarly, the bounds on the dimension of the global attractor given by Constantin, Foias and Temam [11] as well as the lower bounds given by Babin and Vishik [1] all increase as viscosity decreases. Note that these bounds on the dimension of the attractor were shown to be sharp by Ziane [35] for the case of a two-dimensional channel driven by a constant pressure.

Moreover, for calculations of the unforced two-dimensional Navier–Stokes equations in a periodic domain it was observed by Henshaw, Kreiss and Yström in [24] that as the viscosity is decreased somewhat, more modes are required to achieve the same relative error. Since all solutions decay eventually to zero in the unforced case, this study focused on the approximate recovery of the high modes over a transient period of time given a fixed initial condition for the reference calculation. There are many reasons to suppose that the number of numerically determining modes in our experiment should increase as viscosity decreases. However, our numerical results exhibited a different behavior: The number of numerically determining modes stabilized at a finite value as the amplitude γ increased, or equivalently, as ν decreased.

We describe this surprising result in details in Section 2. Note that the differences between our result and the observations reported in [24] can be accounted for by the initial conditions and forcing used for each continuous data assimilation experiment. For each value of ν tested in our work, the reference solution was chosen to lie on the global attractor corresponding to that value of ν. In [24] zero forcing implies that the attractor has been reduced to zero and so a reference solution starting at a fixed non-zero initial condition was used for each value of ν tested.

In Section 3 we examine the role of the non-linear term in continuous data assimilation by performing the same numerical experiment for the linear time-dependent Stokes equations. For a certain range of parameters, the speed with which the approximate solution converges to the reference solution is found to be slower for the Stokes equations than that for the full Navier–Stokes equations. It is commonly believed that the non-linear term is the source of instabilities that compete against the stabilizing effects of the viscous linear term. However, our results indicate that the non-linear term plays an important stabilizing role in the context of continuous data assimilation. This is consistent with the results of Papanicolaou and Fannjiang [14,15] in which it is found that convection significantly enhances diffusion.

Section 4 explains why we preferred an explicit multistep method such as the third-

order Adams–Bashforth method over possibly more accurate and efficient alternatives for our continuous data assimilation experiments. We end by interpreting our numerical observations in terms of the energy represented by the low modes of the energy spectrum.

2. Data Assimilation for the Navier–Stokes Equations

In this section we study how the number of numerically determining modes for the incompressible two-dimensional Navier–Stokes equations depends on the Grashof number.

Let $\Omega = [0, 2\pi]^2$ be the 2π-periodic torus. Following the notation of Constantin and Foias [10], Robinson [31], Temam [33] and our previous work [28], let $\mathcal{V}$ to be the space of L-periodic zero-mean divergence-free $\mathbf{R}^2$-valued trigonometric polynomials defined on Ω whose spatial mean equals zero. Let H be the closure of $\mathcal{V}$ in $L^2(\Omega; \mathbf{R}^2)$, V be the closure of $\mathcal{V}$ in $H^1(\Omega; \mathbf{R}^2)$ and $D(A)$ be the closure of $\mathcal{V}$ in $H^2(\Omega; \mathbf{R}^2)$. Let P_σ be the Leray–Helmholtz orthogonal projection from $L^2(\Omega; \mathbf{R}^2)$ onto H, and let V' be the dual space of V. Furthermore, let $A : V \to V'$ and $B : V \times V \to V'$ be the continuous extensions of the operators such that $Au = -\Delta u$ and $B(u, u) = P_\sigma(u \cdot \nabla u)$ for $u \in \mathcal{V}$. Note that A is also called the Stokes operator.

Each element u of H, V or V' may be represented by a Fourier series of the form

$$u = \sum_{k \in \mathbf{Z}^2 \setminus \{0\}} \hat{u}_k \phi_k,$$

where $\phi_k(x) = e^{ik \cdot x}$ and $\hat{u}_k \in \mathbf{C}^2$ such that $\hat{u}_k = \overline{\hat{u}_{-k}}$ and $k \cdot \hat{u}_k = 0$. In the Fourier representation the norms on H, V and V' are given respectively by $|u| = \|u\|_0$, $\|u\| = \|u\|_1$ and $\|u\|_* = \|u\|_{-1}$, where

$$\|u\|_\alpha = 2\pi \Big\{ \sum_{k \in \mathbf{Z}^2 \setminus \{0\}} |k|^{2\alpha} |\hat{u}_k|^2 \Big\}^{1/2}.$$

Continuous data assimilation is used to find an improved initial condition for weather forecasting on a fine grid given the time history of observational measurements on a coarse grid. In particular, continuous data assimilation obtains an increasingly accurate approximation of a reference solution over time. We shall denote our reference solution by u_1 and our attempt to approximate this solution using continuous data assimilation by u_2. Our study begins by taking u_1 to be the strong solution $u_1 \in L^\infty((0, \infty); V) \cap L^2_{\mathrm{loc}}([0, \infty); D(A))$ to the two-dimensional Navier–Stokes equations given by

$$\frac{du_1}{dt} + \nu_0 A u_1 + B(u_1, u_1) = f \tag{2.1}$$

with $f \in H$ and initial conditions $u_1(0) = u_0 \in V$.

Fourier space provides a convenient way to describe the observational measurements of u_1 needed for our continuous data assimilation experiments. Given $\lambda > 0$ define the orthogonal projections P_λ and Q_λ by

$$P_\lambda a = \sum_{0 < |k|^2 \le \lambda} \hat{a}_k \phi_k \qquad \text{and} \qquad Q_\lambda = I - P_\lambda. \tag{2.2}$$

Then $P_\lambda u_1(t)$ may be viewed as a low-resolution observation of u_1 at time t. Here $\lambda^{-1/2}$ represents the smallest length scale of the solution u_1 which can be observed—the resolution of the measuring equipment.

The approximation u_2 is then obtained by setting $P_\lambda u_2 = P_\lambda u_1$ at each point in time and evolving the high modes $Q_\lambda u_2$ dynamically using the Navier–Stokes equations. In particular, $Q_\lambda u_2$ is computed by

$$\frac{dQ_\lambda u_2}{dt} + \nu_0 A Q_\lambda u_2 + Q_\lambda B(P_\lambda u_1 + Q_\lambda u_2, P_\lambda u_1 + Q_\lambda u_2) = Q_\lambda f \tag{2.3}$$

with initial condition $u_2(0) = P_\lambda u_0$.

Generally, the problem addressed by continuous data assimilation is what to do when we do not know $u_1(0)$. If we knew $u_1(0)$ exactly, then the problem of approximating $u_1(t)$ for $t > 0$ is solved. Here we initialize the high-modes of $u_2(0)$ such that $Q_\lambda u_2(0) = 0$. Similar results would be obtained by setting $Q_\lambda u_2(0) = \eta$ for any $\eta \in Q_\lambda V$.

Let λ_c be the smallest value of λ for which the above algorithm guarantees that $\|u_1 - u_2\| \to 0$ as $t \to \infty$. The best analytic bound on λ_c to date was given in [28] as

$$\lambda_c \le c_1 \min\left\{\mathrm{Gr}(f), c_1 \mathrm{Gr}_*(f)^2\right\} \tag{2.4}$$

where c_1 is a universal constant with $c_1 \le 2 + (2\pi)^{-1}$ and $\mathrm{Gr}(f)$ and $\mathrm{Gr}_*(f)$ are the Grashof number and associated Grashof numbers defined, for example, as in Foias, Jolly, Manley and Rosa [17] by

$$\mathrm{Gr}(f) = \frac{1}{\nu_0^2}|f| \qquad \text{and} \qquad \mathrm{Gr}_*(f) = \frac{1}{\nu_0^2}\|f\|_*.$$

Since the function $\lambda \to \mathrm{card}\{k \in \mathbf{Z}^2 : 0 < |k|^2 \le \lambda\} = \mathrm{rank}(P_\lambda)$ is right continuous, there is a minimal λ_c such that the approximation u_2 obtained by continuous data assimilation of the observations represented by $P_\lambda u_1(t)$ for $\lambda = \lambda_c$ converges to the reference solution u_1 and for any value $\lambda < \lambda_c$ it does not converge to u_1. Define the number of numerically determining modes n_c to be the rank of P_λ for $\lambda = \lambda_c$.

Let $f = \gamma f_0$ where f_0 is forcing function used in [28] for the test case with $\lambda_f = 121$. In particular, $\mathrm{Gr}(f_0) = 250000$, $\mathrm{Gr}_*(f_0) = 23502$ and f_0 is supported on an annulus of Fourier modes such that $10 \le |k| < 12$. Thus, the ratio of the periodic box size to the integral length scale is about 10. This exceeds the ratio of 8 for isotropic turbulence recommended by Pope [30] on page 346. The exact Fourier modes describing f_0 are given in Table 2. Although similar results as presented in this paper should hold for other forcing functions, we felt that it was important to give the exact forcing function here for reference. Further details on how the modes of f_0 were chosen is given in [28].

Note that changing γ is equivalent to varying the viscosity. In particular, setting $\tilde{u}_1(x,t) = (\nu/\nu_0)u_1(x, t\nu/\nu_0)$ where $\gamma = \nu_0^2/\nu^2$ transforms (2.1) into

$$\frac{d\tilde{u}_1}{dt} + \nu A\tilde{u}_1 + B(\tilde{u}_1, \tilde{u}_1) = f_0. \tag{2.5}$$

Thus, our study can also be viewed as an analysis of how the number of numerically determining modes changes as viscosity is decreased.

The initial condition u_0 used for each continuous data assimilation experiment was chosen as in [28] so that it reflects the long term energetics of the forcing. In particular, for each value of γ tested, an initial condition u_0 was obtained by integrating equations (2.1) starting at time $t = -25\,000$ with $u_1(-25\,000) = 0$ until time $t = 0$.

Next, eigenvalues a and b with $a < b$ were found for each γ such that the approximate solution obtained by continuous data assimilation converges to the reference solution for $\lambda = b$ but not for $\lambda = a$. Then continuous data assimilation experiments were performed in parallel for the range of eigenvalues

$$\Lambda(a, b) = \left\{ |k|^2 : k \in \mathbf{Z}^2 \text{ and } |k|^2 \in [a, b] \right\}$$

between a and b to determine the critical value λ_c. These experiments were run from $t = 0$ to $t = 50\,000$. A choice of λ was determined to be sufficient for convergence if by the end of the run the V norm $\|u_1 - u_2\| < 10^{-10}$. In many cases the approximate solution converged to the reference solution with tolerance better than 10^{-14}. Considering $\|u_1\| \approx 1$ and that calculating $\|u_1 - u_2\|$ involves taking the square root of the sum of squares of differences between more that 500 000 floating point numbers each with about 16 digits of precision, our convergence criterion is as close to mathematical convergence as is numerically possible.

Table 1 indicates the values for λ_c found by the numerical simulation of continuous data assimilation for a variety of values of γ. It appears that the number of numerically determining modes stabilizes at a finite value as the Grashof number increases.

The asymptotic result suggested by our computations that the number of determining modes stabilizes at a finite limit with increasing γ, or equivalently, decreasing ν, is surprising. Could it really be that $n_c \to 80$ as $\gamma \to \infty$, or equivalently, as $\nu \to 0$? Common wisdom has been that generically the number of determining modes is a measure of dynamical complexity and that dynamical complexity increases as viscosity decreases. In two dimensions the dissipation length scale is the Kraichnan enstrophy dissipation length scale ℓ_d. Since $\ell_d \to 0$ as $\nu \to 0$ then the heuristic argument that the number of degrees of freedom in two-dimensional turbulence should scale like $(L/\ell_d)^2$ suggests that the number of determining modes should also tend to infinity as $\nu \to 0$. Similarly, Henshaw, Kreiss, Reyna [23] state the resolution necessary to resolve a two-dimensional turbulent flow is

$$\begin{aligned} k_{\max} &= \nu_0^{-1/2} \sup_{\Omega} \left\{ \left| \frac{\partial u}{\partial x} \right|, \left| \frac{\partial v}{\partial x} \right|, \left| \frac{\partial u}{\partial y} \right|, \left| \frac{\partial v}{\partial y} \right| \right\}^{1/2} \\ &= \nu^{-1/2} \sup_{\Omega} \left\{ \left| \frac{\partial \tilde{u}}{\partial x} \right|, \left| \frac{\partial \tilde{v}}{\partial x} \right|, \left| \frac{\partial \tilde{u}}{\partial y} \right|, \left| \frac{\partial \tilde{v}}{\partial y} \right| \right\}^{1/2} \end{aligned}$$

where $u_1 = (u, v)$ and $\tilde{u}_1 = (\tilde{u}, \tilde{v})$. This estimate also tends to infinity as $\nu \to 0$. The values of $k_{\max}$ obtained from our numerical calculations indeed increase as γ increases, or equivalently, as ν decreases. Moreover, we have performed all our calculations using enough Fourier modes to fully resolve $k_{\max}$.

Note that all existing analytic bounds on the number of determining modes are upper bounds. In particular, we have no procedure to obtain a lower bound for the number of determining modes that could be used to check the asymptotic sharpness of the upper

bounds as $\nu \to 0$. Thus, no known analysis provides an obstruction to the hypothesis that the number of determining modes actually stabilizes at a finite limit as $\nu \to 0$. This is in contrast to estimates on the dimension of the global attractor, where linearizing about a steady state and counting the unstable directions gives a lower bound which grows as $\nu \to 0$ and shows the upper bounds are sharp.

In [28] forcing terms were found for the Navier–Stokes equations which led to arbitrarily large Grashof numbers and for which the dynamics of all solutions of the Navier–Stokes equations were trivial. That work indicated the importance of the associated Grashof number in determining the number of determining modes. Still, the analytic bounds given in (2.4) all tend to infinity as $\nu \to 0$. There are three possible scenarios:

1. The number of determining modes is not related to dynamical complexity.
2. The dynamical complexity does not continue to increase as γ increases.
3. We simply have not increased γ enough to see the resulting increase in the number of numerically determining modes.

To address 1 and 2 the notion of dynamical complexity needs to be quantified. Generally we think of dynamical complexity as the degrees of freedom necessary to fully resolve the dynamics in a computation. Although this identification better defines the concept of dynamical complexity, it provides no satisfactory tools for measuring it. At this point and time it is probably best to dodge the issue entirely. Even if the number of numerically determining modes is not directly related to degrees of freedom, it is an important concept on its own because of its association with continuous data assimilation. The number of numerically determining modes indicates how much data is necessary to synchronize two dynamical systems, in this case, two copies of the two-dimensional Navier–Stokes equations. Thus, even if our results do not have a direct relationship to dynamical complexity, they do have a direct relation to the original problem of continuous data assimilation and implications for weather forecasting. In light of this, we rephrase possibility 2 as

2′. The limit of n_c really does stabilize at a finite value as γ increases.

If this is the case, then our results suggest it should be possible to accurately initialize a weather forecasting model using far lower resolution of observational data than pure Reynolds number considerations imply. More energetic turbulence does not necessitate more accurate measurements.

This also means that the convective term is primarily responsible for the convergence of u_2 to u_1 rather than the dissipative term. As all current analysis of the number of determining modes is based on the dissipative term, we conclude that if possibility 2′ is correct, then our theoretical understanding of continuous data assimilation is incomplete. New analytic methods and proofs that make use of the non-linear term need to be found.

It may be, however, that possibility 3 is correct. Keeping in mind the special case given by Machioro [27] of a forcing function for which the corresponding solutions to the Navier–Stokes equations converge to a unique steady state for any $\nu > 0$, perhaps, generally, $n_c \to \infty$ as $\nu \to 0$ and the theoretical bounds in [28], though magnitudes too large, still capture essential qualitative behavior. We have used months of computer time to verify our results for the largest values of γ or equivalently for smallest values of ν that are

practical. Higher Grashof numbers require larger grid sizes and still greater computational investment. The constancy of $n_c = 80$ for over two orders of magnitude in Table 1 is evidence that the number of numerically determining modes stabilizes at 80, not proof. If it is found that $n_c > 80$ for some larger value of γ not currently considered, it is still of interest that n_c was constant for the large range of values computed here.

3. The Role of the Nonlinear Convective Term

To further explore the role of the convective term we drop it and consider continuous data assimilation for the time-dependent linear Stokes equations.

Let v_1 be a solution to the time-dependent linear Stokes equations and v_2 be the approximation of v_1 obtained by continuous data assimilation of the modes $P_\lambda v_1$. Thus,

$$\frac{dv_1}{dt} + \nu_0 A v_1 = f, \quad P_\lambda v_2 = P_\lambda v_1, \quad \text{and} \quad \frac{dQ_\lambda v_2}{dt} + \nu_0 A Q_\lambda v_2 = Q_\lambda f.$$

Since the dynamics of the time-dependent Stokes equations are trivial, then the number of determining modes is zero. In particular, v_2 converges to v_1 for any value of λ. Note also that the absence of non-linearity prevents any coupling between $P_\lambda v_1$ and $Q_\lambda v_2$. Thus, we consider here a question of a different nature: What is the rate of the convergence of the approximate solution to the reference reference solution as $t \to \infty$.

In particular, we take $\lambda > \lambda_c$ and compare the rate of convergence of v_2 to v_1 for the Stokes equations to the rate of convergence of u_2 to u_1 for the Navier–Stokes equations. We use the same viscosity, forcing and initial condition u_0 for both simulations. The results of our computations for $\mathrm{Gr}(f) = 500000$, $\lambda_c = 25$ and $\lambda = 32$ are described in Figure 1. Note that $\mathrm{rank}(P_\lambda) = 100$. As indicated, the rate of convergence of u_2 to u_1 for the Navier–Stokes equation is noticeably faster than the convergence of v_2 to v_1 for the Stokes equations. This suggests that the convective term is largely responsible for the success of continuous data assimilation in the two-dimensional Navier–Stokes equations.

Although the convective term does nothing but hinder us in the proof of (2.4), its role numerically is different. We observe, based on our simulations, that the rate of convergence for continuous data assimilation in the Navier–Stokes equations is faster than for the Stokes equations. Thus, the convective term seems to play an important and stabilizing role in practice. Only when we obtain a proof of the convergence of continuous data assimilation that uses these properties of the nonlinear term will we be able to obtain a sharp upper bound for the number of determining modes. In [24] Henshaw, Kreiss and Yström state the following conjecture:

> *The large-scale modes determine the basic structure of the flow and set up the dissipative structures.... The large-scale motion advects perturbations towards the dissipative structures, where they are compressed and transformed into higher frequencies which can be effectively dissipated by viscous effects.*

Intuitively, as ν decreases the non-linear term dominates the inertial range. Since the non-linear term appears to be crucially involved in the convergence of u_2 to u_1, it is possible that the number of numerically determining modes really does stabilize at some finite value as γ increases. This is what our computations seem to indicate.

It is interesting to note that using different techniques Papanicolaou and Fannjiang [14,15] also obtain that convection enhances diffusion in turbulent flows. This further supports the mechanism for continuous data assimilation conjectured by Henshaw, Kreiss and Yström [24] in which the nonlinear coupling between the large and small-scale motion can increase the effective dissipation of the error.

Returning to the Navier–Stokes equations we compute average energy spectra for different values of the Grashof number. Our results are given in Figure 2. Note that the decrease in number of numerically determining modes from 108 to 80 coincides to a buildup of energy in the lowest modes of the calculation. This buildup is related to the fact that in 2D flows there is a forward cascade of enstrophy and an inverse cascade of energy. Note that for each continuous data assimilation experiment we have chosen our initial condition u_0 by integrating the Navier–Stokes equations over a period of time sufficiently long to obtain a statistically equilibrium state. In particular, this means the buildup of energy in the low modes has equilibrated. Since we have not employed hypoviscosity to remove additional energy from the low modes, reaching this equilibrium requires a significant amount of computational time for large Grashof numbers. The result is that for large Grashof numbers the energy in the $|k| = 1$ energy shell is more than 100 times the energy in the $|k| = 11$ energy shell; whereas, for small Grashof numbers the energy in the $|k| = 1$ energy shell is less than the energy in the $|k| = 11$ energy shell.

For the unforced case with a fixed initial condition, Eyink [13] showed that solutions to the Navier–Stokes equations tend to a weak solution of the Euler equations as $\nu \to 0$ provided $\tilde{E}(k) = (\nu/\nu_0)E(k)$ is bounded by the Kraichnan–Batchelor k^{-3} spectrum uniformly for $\nu > 0$. Lopes Filho, Mazzucato and Nussenzveig Lopes [16] extend some of Eyink's results and provide an example in which the enstrophy transport defect is zero but the viscous enstophy defect is positive. Dritchel, Tran and Scott [12] provide numerical evidence showing that the rate of enstrophy dissipation tends to zero as $\nu \to 0$. Moreover, in all these works it is observed that the rate of enstrophy dissipation vanishes in the limit $\nu \to 0$ provided the limit flow has finite enstrophy and supremum of vorticity.

In the forced case considered here, a different initial condition u_0 was chosen for each value of ν studied. Since the global attractor expands as $\nu \to 0$, then the norm of u_0 almost surely tends to infinity as $\nu \to 0$. Thus, our limit can not be used to obtain a viscosity solution of the Euler equations, and in particular, doesn't imply that the Euler equations possess a finite number of determining modes. At the same time, it may be possible to relate the stabilization of the number of numerically determining modes as $\nu \to 0$ observed here to the dissipation anomaly conjectured by Orszag [29] and Batchelor [2] for viscosity solutions of the Euler equations. This difficult task we do not embark upon.

We end this section by comparing the vorticity field for a flow with $\mathrm{Gr}(f) = 50\,000$ to a flow with $\mathrm{Gr}(f) = 750\,000$. Level curves of representative vorticity fields are plotted in Figures 3 and 4 respectively. Note the flow for $\mathrm{Gr}(f) = 750\,000$ has noticeably more large scale structure compared to the flow for $\mathrm{Gr}(f) = 50\,000$. Indeed, the dominant features of Figure 4 are a large positive eddie in the upper-left corner and a negative one in the lower-right corner whereas Figure 3 has no such distinctive features. This is consistent with the energy spectra in Figure 2 where most of the energy is in the lowest modes, that is, in the large spatial scales and eddies when the Grashof number is large. Again note that we have not employed hypoviscosity to dissipate these large eddies as, for example, in

Chen, Ecke, Eyink, Wang and Xiao [8]. Figures 3 and 4 suggest that as $\mathrm{Gr}(f)$ increases the motion of the resulting two large eddies play a significant role in determining the higher modes of solutions of the Navier–Stokes equations.

4. Numerical Methods

Computations were carried out using a C code written by the authors in conjunction with the Fourier transform library of Frigo and Johnson [21]. This code employs a spectral Galerkin method and integrates in time using a third order Adams–Bashforth (AB) method that reproduces the dissipative term exactly. Further details of this code appear in [28].

The actual calculations were performed at the University of Nevada, Reno using the PDEWulf Beowulf cluster in the Department of Mathematics. This cluster consists of 30 nodes running the GNU/Linux operating system and LAM/MPI connected by fast ethernet. During each continuous data assimilation run a reference solution u_1 was calculated on one node while continuous data assimilation approximations for different values of λ were calculated in parallel on additional nodes. At each time step t_n the data representing $P_\lambda u_1(t_n)$ was transmitted using LAM/MPI from the first node to each of the additional nodes. Due to the one-way flow of buffered data and the small number of modes represented by $P_\lambda u_1(t_n)$ this resulted in an efficient computation with almost no time spent waiting on node to node communication. Hence a run using $N+1$ computational nodes could quickly check N different values of λ in parallel.

Computations were performed with $L = 2\pi$ and $\nu_0 = 0.0001$. To avoid aliasing the 2/3 rule was used (see, for example, Canuto, Hussaini, Quarteroni and Zang [5]). Thus, Fourier transforms performed on a 512^2 grid resulted in a 341^2 mode spectral Galerkin method. For an N^2 Fourier transform the largest resolved wave number is about $N/3$. In all cases, grid sizes were chosen so that $k_{\max} < N/3$. In particular, for higher Grashof numbers Fourier transforms were performed using 768^2 and 1024^2 modes. Finally, the time step Δt was chosen to ensure that the CFL condition

$$\mathrm{CFL} = \frac{n\Delta t}{2L} \sup_{(x,y)\in\Omega} \big\{ |u(x,y)| + |v(x,y)| \big\} \leq 1$$

was satisfied throughout the run.

It is worth mentioning why we chose an Adams–Bashforth method as opposed to a more efficient implicit or Runge–Kutta (RK) method. For general computation a different time integration method could have a larger domain of stability, smaller truncation error and be more efficient. However, for the continuous data assimilation experiments performed here, an explicit multistep method with a single functional evaluation per time step is preferred.

Consider a time discretization at the points t_n in time. We say that the dynamics of a single-step method are identical if $u_1(t_n) = u_2(t_n)$ implies $u_1(t_{n+1}) = u_2(t_{n+1})$ for each n. Similarly, identical dynamics for a s-step multistep method means for each n that $u_1(t_{n+1}) = u_2(t_{n+1})$ whenever $u_1(t_j) = u_2(t_j)$ for $j = n-s+1, \ldots, n$. The numerical properties we wanted our method to possess were

1. Only the information $P_\lambda u_1$ should be used in the computation of u_2.

2. The discrete dynamics of u_1 and u_2 should be identical.

3. The method should be of order greater than 1.

As we shall show, no implicit or RK method can satisfy 1, 2 and 3.

To see this, note that we are solving a system of coupled equations of the form

$$\begin{aligned} u_1' &= f(u_1) \\ u_2' &= g(u_2, P_\lambda u_1). \end{aligned}$$

Since u_1 depends on time, then the equation governing the evolution of u_2 may be viewed on its own as non-autonomous. Moreover, as the values of $P_\lambda u_1$ are available only at the times t_n computed by the first computer, this makes it is difficult to evaluate g on a second computer at intermediate times often used in RK stages.

One might try to evaluate g at times between time steps by interpolating $P_\lambda u_1$ or by computing u_1 using smaller time steps than for u_2. Either method results in non-identical dynamics for u_1 and u_2. Note that only by ensuring the dynamics of u_1 and u_2 are identical do we obtain the convergence of $\|u_1 - u_2\|$ to zero with the near machine precision demonstrated in our calculations. Moreover, identical discrete dynamics avoids trouble that can come from coupling two mismatched systems.

Unfortunately, even if the RK stages are chosen to employ only the times t_n, it is impossible to keep the discrete dynamics of u_1 and u_2 identical. We encounter similar difficulties for implicit methods. In fact, any time integration method that evaluates g more than once per time step has trouble satisfying properties 1–3 above.

For example, consider the RK2 method for computing u_2 given by

$$\begin{aligned} k_1 &= hg(u_2(t_n), P_\lambda u_1(t_n)) \\ k_2 &= hg(u_2(t_n) + k_1, P_\lambda u_1(t_{n+1})) \\ u_2(t_{n+1}) &= u_2(t_n) + (k_1 + k_2)/2. \end{aligned}$$

Here one uses the measurement values of $P_\lambda u_1(t_{n+1})$ for the computation of k_2. If u_1 is also computed by RK2, then the discrete dynamics of u_2 will be different than u_1. In particular if $u_1(t_n) = u_2(t_n)$ then u_2 has a predictor corrector flavor to it. It follows that $u_1(t_{n+1}) \neq u_2(t_{n+1})$. Thus, property 2 is not satisfied. One could fix this by writing

$$\begin{aligned} k_1 &= hg(u_2(t_n), P_\lambda u_1(t_n)) \\ k_2 &= hg(u_2(t_n) + k_1, P_\lambda (u_2(t_n) + k_1)) \\ u_2(t_{n+1}) &= u_2(t_n) + (k_1 + k_2)/2. \end{aligned}$$

However, this is inconsistent with the continuous aspect of the continuous data assimilation and effectively makes the continuous data assimilation part of the calculation first order. Thus, it does not satisfy property 3.

The only alternative is coupling each stage of the RK method as well to obtain

$$\begin{aligned} l_1 &= hf(u_1(t_n)) \\ l_2 &= hf(u_1(t_n) + l_1) \\ k_1 &= hg(u_2(t_n), P_\lambda u_1(t_n)) \\ k_2 &= hg(u_2(t_n) + k_1, P_\lambda (u_1(t_n) + l_1)) \\ u_2(t_{n+1}) &= u_2(t_n) + (k_1 + k_2)/2. \end{aligned}$$

However, this requires plugging the low modes of the intermediate RK stages of the reference calculation l_1 into the calculation of u_2 as well as the measurements $P_\lambda u_1(t_n)$. This violates property 1 and appears less physical.

To satisfy properties 1–3 we use an explicit multistep method for our continuous data assimilation calculations. Note that we integrate the viscosity term exactly which helps overcome some of the drawbacks related to stability of the AB methods with respect to the viscous term. The exact numerical scheme is described in [28].

5. Conclusion

The number of determining modes was numerically measured for a particular forcing function $f = \gamma f_0$ scaled with different values of γ ranging from $\mathrm{Gr}(f) = 12\,500$ to $60\,000\,000$. The number of numerically determining modes increased to 108 at $\mathrm{Gr}(f) = 125\,000$ and after that decreased to 80. In terms of the rescaled version (2.5) of the two-dimensional Navier–Stokes equations increasing γ is equivalent to decreasing ν.

Let us model the energy spectrum for the Navier–Stokes equations by

$$E(k) \approx Ck^{-\beta}e^{-\alpha k}$$

where β is independent of ν and C and α depend on ν with $\alpha \to 0$ as $\nu \to 0$. Such model spectra are justified by the Gevrey class regularity results shown by Foias and Temam [20] for solutions to the two-dimensional Navier–Stokes equations, see also [22] where Gevrey regularity is used to show exponential convergence of the Galerkin method for Bénard convection in porous media.

For ν small enough our numerical results suggest that the energy E_{det} present in the determining modes is given by

$$E_{\mathrm{det}} = \sum_{k=1}^{25} E(k).$$

Moreover, provided $\beta > 1$ we have

$$\frac{E_{\mathrm{det}}}{E} \approx \frac{\sum_{k=1}^{25} k^{-\beta}e^{-\alpha k}}{\sum_{k=1}^{\infty} k^{-\beta}e^{-\alpha k}} \to R \quad \text{as} \quad \nu \to 0$$

where

$$R = \frac{\sum_{k=1}^{25} k^{-\beta}}{\sum_{k=1}^{\infty} k^{-\beta}}$$

is non-zero fixed ratio.

Thus, our observation that the number of numerically determining modes stabilizes at 80 as $\nu \to 0$ is consistent with the statement that the lowest modes containing a certain fixed percentage of the total energy are sufficient to determine the flow. Viewed in this way our results are plausible. Note that similar arguments apply to more detailed model spectra, for example, the model spectra discussed in Pope [30] on page 232.

An interesting byproduct of our calculations is the observation in Figure 2 of the effects of an inverse cascade of energy through the buildup of energy in the low modes when ν

is small. It would be interesting to test to what extent the large box-size eddies resulting from this buildup are essential for our numerical results on determining modes. In [11] and [35] the fractal dimension of the global attractor for the two-dimensional Navier–Stokes equations was shown to be of the order $\mathcal{O}(\nu^{-4/3})$ as $\nu \to 0$. In [25] the dimension of the attractor for the damped two-dimensional Navier–Stokes equations

$$\frac{du}{dt} + \nu Au + \mu u + B(u,u) = f_0$$

holding $\mu > 0$ fixed was shown to be of the order $\mathcal{O}(\nu^{-1})$ as $\nu \to 0$. As seen by the change in the fractal dimension of the global attractor, the damping term seriously alters the dynamics of the Navier–Stokes equations. This damping is a form of hypoviscosity. It is motivated by the Rayleigh friction present in the Stommel–Charney model of ocean circulation [6,32] and acts as a sink to dissipate energy at the large scales. A study on whether the number of determining modes stabilize as $\nu \to 0$ in a modified Navier–Stokes model that employs hypoviscosity to damp the large eddies is planned as future work.

We end by emphasizing the necessity of new mathematical analysis which makes good use of the non-linear term to fully understand continuous data assimilation and the number of numerically determining modes for the two-dimensional Navier–Stokes equations.

6. Acknowledgements

The work of E.O. was supported in part by a grant from the University of Nevada, Reno, Junior Faculty Research Grant Fund. The work of E.S.T was support in part by NSF grant number DMS–0504619, BSF grant number 2004271 and ISF grant number 120/6.

7. References

[1] A.V. Babin, M.I. Vishik, Attractors of evolution partial differential equations and estimates of their dimension (Russian), *Uspekhi Mat. Nauk* **38** (1983), 141–213.

[2] G.K. Batchelor, Computation of the energy spectrum in homogeneous two-dimensional turbulence, *Phys. Fluids Suppl. II* **13** (1969), 233–239.

[3] G.L. Browning, W.D. Henshaw, H.O. Kreiss, A numerical investigation of the interaction between the large and small scales of the two-dimensional incompressible Navier–Stokes equations, UCLA CAM Technical Report 98-23.

[4] G.L. Browning, W.D. Henshaw, H.O. Kreiss, A numerical investigation of the interaction between the large and small scales of the two-dimensional incompressible Navier–Stokes equations, Research report LA-UR-98-1712, Los Alamos National Laboratory, Los Alamos, NM, 1998.

[5] C. Canuto, M.Y. Hussaini, A. Quarteroni, T.A. Zang, *Spectral Methods in Fluid Dynamics*, Springer Series in Computational Physics, Springer-Verlag, 1988.

[6] J. Charney, The Gulf Stream as an inertial boundary layer, *Proc. Nat. Acad. Sci.* **41** (1955), 731–740.

[7] J. Charney, M. Halem, R. Jastrow, Use of incomplete historical data to infer the present state of the atmosphere, *J. Atmos. Sci.* **26** (1969) 1160–1163.

[8] S. Chen, R.E. Ecke, G.L. Eyink, X. Wang, Z. Xiao, Physical mechanism of the two-dimensional enstrophy cascade, *Phys. Rev. Lett.* **91**:214501 (2003), 1–4.

[9] B. Cockburn, D.A. Jones, E.S. Titi, Determining degrees of freedom for nonlinear dissipative equations, *C. R. Acad. Sci. Paris Sér. I Math.* **321**:5 (1995), 563–568.

[10] P. Constantin, C. Foias, *Navier-Stokes Equations*, The University of Chigaco Press, 1988.

[11] P. Constantin, C. Foias, R. Temam, On the dimension of the attractors in two-dimensional turbulence, *Physica D* **30** (1988), 284–296.

[12] D.G. Dritschel, C.V. Tran, R.K. Scott, Revisiting Batchelor's theory of two-dimensional turbulence, preprint.

[13] G.L. Eyink, Dissipation in turbulent solutions of 2D Euler equations, *Nonlinearity* **14** (2001) 787–802.

[14] A. Fannjiang, G. Papanicolaou, Convection enhanced diffusion for periodic flows, *SIAM J. Appl. Math.* **52**:2 (1994), 333–408.

[15] A. Fannjiang, G. Papanicolaou, Convection enhanced diffusion for random flows, *J. Statist. Phys.* **88**:5–6 (1997), 1033–1076.

[16] M.C. Lopes Filho, A.L. Mazzucato, H.J. Nussenzveig Lopes, Weak solutions, renormalized solutions and enstophy defects in 2D turbulence, preprint.

[17] C. Foias, M.S. Jolly, O.P. Manley, R. Rosa, Statistical estimates for the Navier–Stokes equations and the Kraichnan theory of 2D fully developed turbulence, *Journal of Statistical Physics* **108** (2002), 591–645.

[18] C. Foias, O. Manley, R. Rosa, R. Temam, *Navier–Stokes Equations and Turbulence*, Encyclopedia of Mathematics and It's Applications, Vol 83, Cambridge University Press, 2001.

[19] C. Foias, G. Prodi, Sur le comportement global des solutions non stationnaires des équations de Navier–Stokes en dimension two, *Rend. Sem. Mat. Univ. Padova*, **39** (1967), 1–34.

[20] C. Foias, R. Temam, Gevrey class regularity for the solutions of the Navier-Stokes equations. *J. Funct. Anal.* **87**:2 (1989), 359–369.

[21] M. Frigo, S.G. Johnson, The Fastest Fourier Transform in the West, MIT Technical Report, MIT-LCS-TR-728, `http://www.fftw.org/`, 1997.

[22] M.D. Graham, P.H. Steen, E.S. Titi, Computational efficiency and approximate inertial manifolds for a Beńard convection system. *J. Nonlinear Sci.* **3**:2 (1993), 153–167.

[23] W.D. Henshaw, H.O. Kreiss and L.G. Reyna, On the smallest scale for the incompressible Navier–Stokes equations, *Theor. Comp. Fluid Dynam.* **1** (1989) 65–95.

[24] W.D. Henshaw, H.O. Kreiss, J. Ystrröm, Numerical experiments on the interaction between the large and small-scale motions of the Navier-Stokes equations, *Multiscale Model. Simul.* **1**:1 (2003), 119–149.

[25] A.A. Ilyin, A. Miranville, E.S. Titi, Small viscosity sharp estimates for the global attractor of the 2-D damped-driven Navier-Stokes equations, *Commun. Math. Sci.* **2**:3 (2004), 403–426.

[26] D. Jones, E.S. Titi, Upper bounds on the number of determining modes, nodes, and volume elements for the Navier–Stokes equations, *Indiana Univ. Math. J.* **42**:3 (1993), 875–887.

[27] C. Marchioro, An example of absence of turbulence for any Reynolds number, *Comm. Math. Phys.*, **105**:1 (1986), 99–106.

[28] E. Olson, E.S. Titi, Determining modes for continuous data assimilation in 2D turbulence, *Journal of Statistical Physics* **113**:516 (2003), 799–840.

[29] S.A. Orszag, Analytical theories of turbulence, *J. Floid Mech* **41** (1970), 363–386.

[30] S.B. Pope, *Turbulent Flows*, Cambridge University Press, 2000.

[31] J. Robinson, *Infinite-Dimensional Dynamical Systems*, Cambridge Texts in Applied Mathematics, 2001.

[32] H. Stommel, The westward intensification of wind-driven ocean currents, *Trans. Amer. Geophys. Union* **29** (1948), 202–206.

[33] R. Temam, *Navier–Stokes Equations and Nonlinear Functional Analysis*, CBMS-NSF Regional Conference Series in Applied Mathematics, 1995.

[34] R. Temam, *Infinite Dimensional Dynamical Systems in Mechanics and Physics*, 2nd edition, Springer–Verlag, New York, 1997.

[35] M. Ziane, Optimal bounds on the dimension of attractors for the Navier–Stokes equations, *Physica D* **105** (1997), 1–19.

TABLE 1. Values of λ_c and n_c for different Grashof numbers. Here FFT indicates the size of the Fourier transforms, Δt the time step, $\mathrm{CFL}_{\max}$ the maximum CFL number and $k_{\max}$ the maximum value of Kreiss's upper bound on the magnitude of the largest mode needed to resolve the flow over the entire run.

$\mathrm{Gr}(f)$	FFT	Δt	$\mathrm{CFL}_{\max}$	$k_{\max}$	λ_c	n_c
12 500	512^2	0.16	0.2362	20.2	0	0
25 000	512^2	0.16	0.4188	28.9	8	24
37 500	512^2	0.16	0.7083	34.8	20	68
50 000	512^2	0.16	0.9467	40.8	26	88
62 500	512^2	0.08	0.2757	45.8	29	96
125 000	512^2	0.01	0.1217	60.0	34	108
250 000	512^2	0.01	0.2061	74.7	26	88
500 000	512^2	0.01	0.3328	104.4	25	80
750 000	512^2	0.01	0.4569	99.6	25	80
1 000 000	512^2	0.01	0.5453	113.6	25	80
1 250 000	512^2	0.005	0.3276	112.7	25	80
1 500 000	512^2	0.005	0.3892	123.0	25	80
1 750 000	512^2	0.005	0.4280	123.6	25	80
2 000 000	512^2	0.005	0.4380	137.4	25	80
2 500 000	512^2	0.005	0.5161	129.1	25	80
3 000 000	512^2	0.005	0.5663	148.8	25	80
4 000 000	512^2	0.005	0.7060	164.6	25	80
6 000 000	768^2	0.00125	0.3455	178.7	25	80
8 000 000	768^2	0.00125	0.4452	189.3	25	80
12 000 000	768^2	0.00125	0.5302	227.2	25	80
16 000 000	768^2	0.00125	0.7002	257.1	25	80
24 000 000	1024^2	0.000625	0.5016	262.8	25	80
36 000 000	1024^2	0.000625	0.7345	332.6	25	80
48 000 000	1024^2	0.0003125	0.4303	344.2	25	80
60 000 000	1024^2	0.0003125	0.4984	378.8	25	80

TABLE 2. Fourier modes for $g_0 = \nabla \times f_0$. Since the reality condition implies $\hat{g}_{-k} = \overline{\hat{g}_k}$ we list only half the modes here.

k	$\hat{g}_k \times 10^{-4}$	k	$\hat{g}_k \times 10^{-4}$
$(4,11)$	$-1.68185 - 1.37884i$	$(10,0)$	$1.24568 + 0.999582i$
$(3,11)$	$-0.501504 - 4.39707i$	$(11,0)$	$-2.45397 - 2.1001i$
$(-11,1)$	$3.22868 + 3.57232i$	$(-10,1)$	$-3.6533 + 4.34302i$
$(10,1)$	$-0.168267 + 3.63812i$	$(11,1)$	$1.74878 + 0.537828i$
$(-11,2)$	$1.83238 + 4.56593i$	$(-10,2)$	$-2.27939 + 5.32842i$
$(10,2)$	$1.08206 - 2.65437i$	$(11,2)$	$-0.12495 - 0.439438i$
$(-11,3)$	$1.23101 + 2.32092i$	$(-10,3)$	$3.24541 - 2.56086i$
$(10,3)$	$-4.36393 + 4.81623i$	$(11,3)$	$-3.25672 - 2.04313i$
$(-11,4)$	$0.772188 - 2.22768i$	$(-10,4)$	$-1.18464 + 3.6144i$
$(10,4)$	$0.352859 + 3.8498i$	$(11,4)$	$-0.0779563 - 0.483413i$
$(-10,5)$	$2.95066 - 3.88721i$	$(-9,5)$	$1.43467 - 3.13185i$
$(9,5)$	$-4.65628 - 0.853542i$	$(10,5)$	$-0.678476 + 1.56749i$
$(-10,6)$	$2.14982 + 3.9452i$	$(-9,6)$	$0.794682 - 0.405619i$
$(-8,6)$	$0.847957 + 6.09509i$	$(8,6)$	$0.412921 + 1.72437i$
$(9,6)$	$-0.933718 + 1.34388i$	$(10,6)$	$-0.960698 + 1.73383i$
$(-9,7)$	$3.75659 - 1.43354i$	$(-8,7)$	$-2.33465 - 1.91763i$
$(8,7)$	$-3.07828 + 1.434i$	$(9,7)$	$-1.4385 + 2.08662i$
$(-8,8)$	$1.57689 - 3.96814i$	$(-7,8)$	$-0.206682 + 2.31327i$
$(-6,8)$	$0.689446 - 2.66231i$	$(6,8)$	$-0.956604 - 2.33234i$
$(7,8)$	$2.87397 - 1.28323i$	$(8,8)$	$0.140247 + 0.118369i$
$(-7,9)$	$3.06962 + 1.30303i$	$(-6,9)$	$2.42145 - 0.448085i$
$(-5,9)$	$1.3582 - 2.86109i$	$(5,9)$	$-3.58454 + 1.92307i$
$(6,9)$	$-1.08488 - 0.661055i$	$(7,9)$	$2.62845 + 3.4255i$
$(-6,10)$	$0.178138 - 2.35925i$	$(-5,10)$	$1.83893 + 3.99093i$
$(-4,10)$	$-1.30734 - 1.20256i$	$(-3,10)$	$3.46985 + 0.165801i$
$(-2,10)$	$-4.54014 + 2.54287i$	$(-1,10)$	$-1.81676 - 6.38674i$
$(0,10)$	$2.28551 - 4.28632i$	$(1,10)$	$4.89391 - 0.112915i$
$(2,10)$	$-2.75146 + 0.206303i$	$(3,10)$	$-2.18555 - 0.921325i$
$(4,10)$	$0.0705579 - 0.807738i$	$(5,10)$	$1.54712 - 1.76146i$
$(6,10)$	$1.97628 - 1.26563i$	$(-4,11)$	$-4.18572 - 0.412749i$
$(-3,11)$	$4.63344 + 3.9968i$	$(-2,11)$	$0.161582 + 4.15786i$
$(-1,11)$	$3.03338 - 1.77921i$	$(0,11)$	$-0.608278 - 1.09338i$
$(1,11)$	$-3.64792 + 6.35805i$	$(2,11)$	$1.35454 - 1.92183i$

FIGURE 1. Comparison of the rate of continuous data assimilation on $n = 100$ modes between the Navier–Stokes equations and the Stokes equations for $\mathrm{Gr}(f) = 500000$.

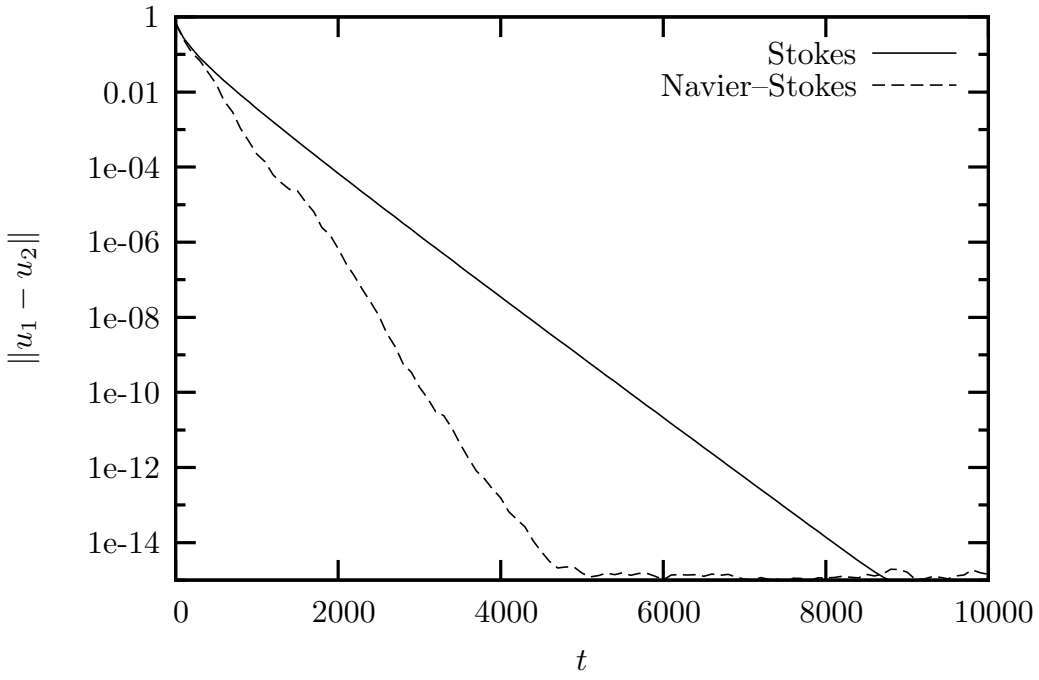

FIGURE 2. Comparison of the energy spectra averaged from $t = 0$ to 10 000 for representative Grashof numbers. Note that for the two largest Grashof numbers there is a significant amount of energy in the lowest modes.

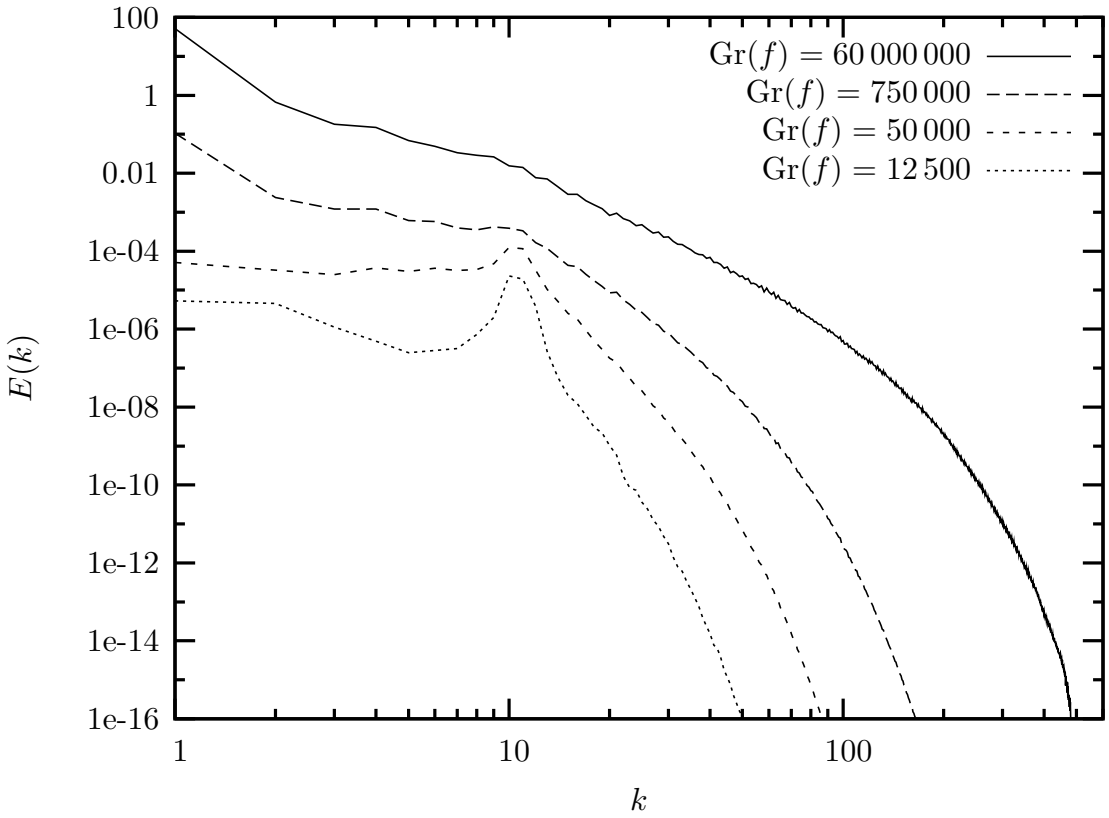

FIGURE 3. Level curves of the vorticity field at time $t = 5000$ corresponding to the Grashof number $\mathrm{Gr}(f) = 50\,000$. The eddies in this flow are of size comparable to the scales present in the forcing.

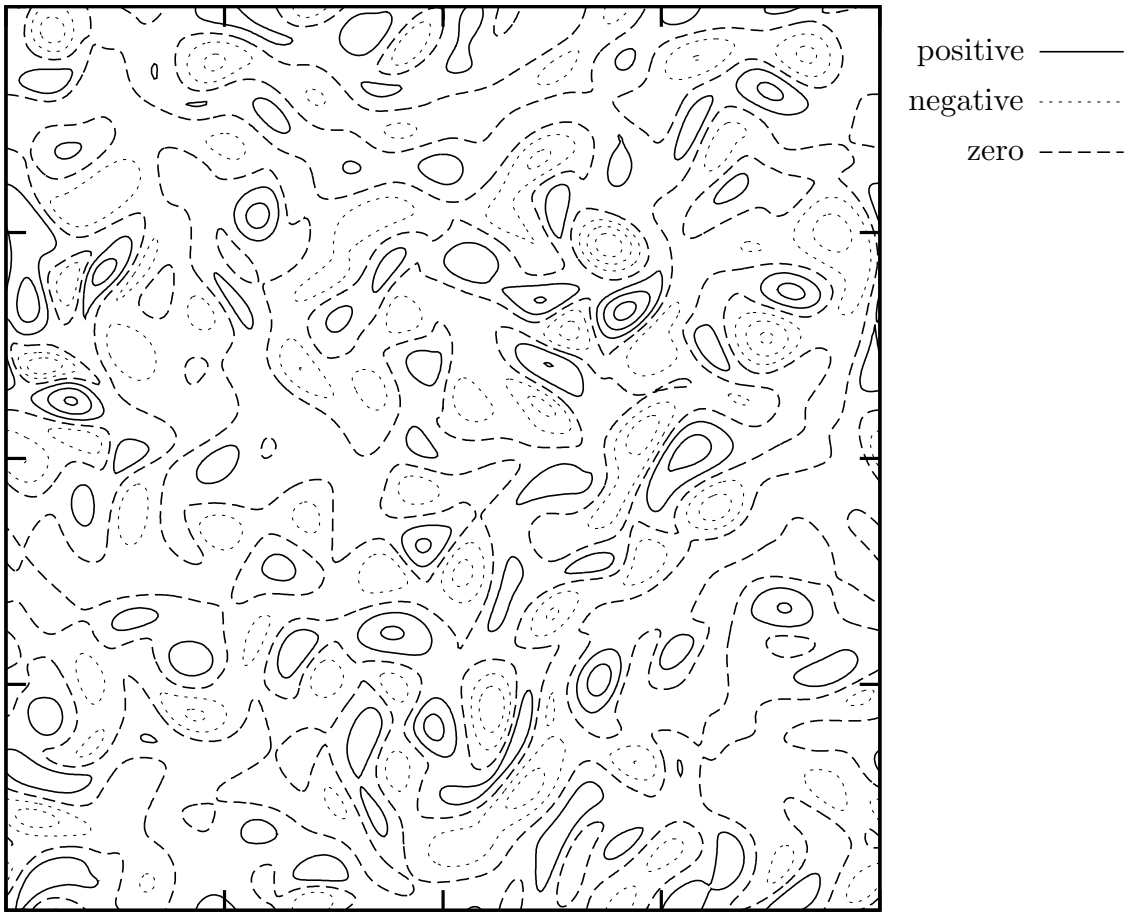

FIGURE 4. Level curves of the vorticity field at time $t = 5000$ corresponding to the Grashof number $\mathrm{Gr}(f) = 750\,000$. The two large eddies in this flow are at scales 10 times larger than present in the forcing.